# Resiliency Enhancement and Power Quality Optimization of Converter-Based Renewable Energy Microgrids

Mohammad Sadegh Eslahi, Sadegh Vaez-Zadeh, *Senior Member, IEEE*, and Jose Rodriguez, *Life Fellow, IEEE*

***Abstract*—The converter-based renewable energy microgrids are becoming indispensable parts of power grids. Nevertheless, the increasing risks by different causes deteriorate the resiliency of their grid integration. In this article, a sensorless combined control method for the grid-connected converters is proposed to enhance the resiliency in different aspects and against multiple risks. Power quality improvement is also considered in the proposed method, along with enhancing resiliency. A single control system is proposed to deal with unbalanced grid conditions, severe load changes, and short circuit faults. The control system has a low dependence on the system parameters. Also, a new reference calculation is proposed to improve the system performance under balanced and unbalanced conditions. It provides stable operation under normal and abnormal conditions, such as unbalanced voltages, voltage sag, faults, etc. The operation under the proposed control system is compared with the one under a conventional control system to confirm its performance superiority through simulation and experimental results.**

***Index Terms*—Combined control (CC), current control, faults, grid connection, resilience, risks, sensorless, unbalanced voltages, virtual flux (VF), voltage source converters.**

## Nomenclature

| | |
|---|---|
| $e$, $v$ | Grid and converter voltage vectors. |
| $i$ | Grid current vector. |
| $R$, $L$ | Equivalent series resistance and inductance. |
| $P$, $Q$ | Active and reactive powers. |
| $\lambda_e$, $\lambda_v$, $\lambda_{cap}$ | Grid, converter, and capacitor flux linkage. |
| $\omega$ | Angular frequency of grid voltage. |
| $\delta_e$ | Grid voltage angle. |
| $I_f$, $I_h$ | Fundamental and harmonic current components. |
| $A_c$, $B_c$, $C_c$, $E_c$ | System matrices. |
| $P_{\text{nom}}$ | Nominal active power capacity of the converter. |
| $V_{\text{PCC}}$ | Voltage at point of common connection. |
| $i_e$, $i_v$, $i_{\text{cap}}$ | Grid, converter side, and capacitor currents in *LCL* topology. |
| *Superscripts* | |
| $*$ | Reference value. |
| $'$ | 90 electrical degrees lagged vectors. |
| *Subscripts* | |
| $\alpha\beta$ | Stationary $\alpha$, $\beta$ axis. |
| *dq* | Synchronously rotating *d*, *q* axis. |
| *xy* | Grid virtual flux *x*, *y* axis. |
| *0, c, s* | DC, cosine, and sine components. |
| $+$, - | Positive and negative sequence of a vector. |
| *dis* | Discrete-time model. |
| *Acronyms* | |
| GCC | Grid-connected converter. |
| VC | Vector control. |
| DPC | Direct power control. |
| CC | Combined control. |
| VF | Virtual flux. |
| THD | Total harmonic distortion. |
| LVRT | Low-voltage right-through. |

Manuscript received 11 August 2022; revised 24 December 2022 and 28 February 2023; accepted 3 March 2023. Date of publication 14 March 2023; date of current version 20 April 2023. This work was supported in part by the Iran National Science Foundation under Project 940013, and in part by ANID under Projects FB0008, 1210208, and 1221293. Recommended for publication by Associate Editor F.-J. Lin. *(Corresponding author: Sadegh Vaez-Zadeh.)*

Mohammad Sadegh Eslahi is with the School of Electrical and Computer Engineering, College of Engineering, University of Tehran, Tehran 1481954953, Iran (e-mail: mseslahi@ut.ac.ir).

Sadegh Vaez-Zadeh is with the Advanced Motion Systems Research Laboratory, School of Electrical and Computer Engineering, College of Engineering, University of Tehran, Tehran 14395-515, Iran (e-mail: vaezs@ut.ac.ir).

Jose Rodriguez is with the Universidad San Sebastian, Santiago 8420524, Chile (e-mail: jose.rodriguezp@uss.cl).

Color versions of one or more figures in this article are available at https://doi.org/10.1109/TPEL.2023.3257084.

Digital Object Identifier 10.1109/TPEL.2023.3257084

## I. Introduction

IT IS predicted that the global share of renewable energy in the power sector will increase to 85% by 2050 [1]. Converter-based renewable power plants in microgrids would mainly generate it. The increasing penetration level of renewable energy in power grids provides major challenges in grid integration. In fact, the increasing risks by different causes, from natural disasters to cyber-attacks, deteriorate the resiliency of grid integration of renewable microgrids. The control method applied to the converter-based renewable microgrids is an opportunity to overcome the integration challenge. It should guarantee the stability, reliability, and resiliency of the microgrids according to advanced grid codes under normal and abnormal conditions [2], [3]. Besides many methods that have been provided for the control of microgrids under normal conditions, various control methods have been proposed to overcome the problems of grid unbalanced conditions for single and three-phase converts [4], [5]. Also, different methods have been proposed to enhance the LVRT capability during faults [6], [7]. However, a few

studies could be found in which 1) a control system successfully faces multiple risks simultaneously and enhance the resiliency in different aspects, 2) the power quality is improved, and 3) the system experiences little dependence on the parameters. It is desirable to tackle the challenges with a single converter control system.

Most high-capacity renewable power plants are located at long distances from load centers. Therefore, the probability of occurrence of events with low probability and high impact is increased and inevitable. The consequences of such events can range from local problems to power system collapse, and power quality derates, etc. Generally, these kinds of events could be classified into the following categories [8], [9], [10].

1) Technical issues, such as unbalanced conditions, symmetrical and asymmetrical faults, etc.
2) Equipment failures or malfunctions.
3) Cyber, physical, or cyber-physical sabotages.

Therefore, more accurate and advanced control systems are needed to guarantee the system resiliency before, during, and following such disturbances.

Generally, the GCC control methods can be categorized into pulsewidth modulation (PWM) based and table-based methods. Different analytical and experimental studies show that VC is the most known PWM-based method. It inherently enjoys good steady-state, dynamic performance, and constant switching frequency. However, a feedforward circuit and thus its dependence on the system parameters are the VC disadvantages. Also, in VC, the PI controllers tuning to have a good performance for a wide range of operations are a challenge [11]. DPC is the most famous table-based method. DPC regulates the active and reactive power faster than VC with a simple structure. Also, DPC is more robust against grid and filter parameter variations than VC. However, designing filters and attenuating certain harmonics in the DPC method is more complicated than in VC due to a variable switching frequency [12]. CC is proposed to integrate the positive features of VC and DPC in a control system. As a table-based method, CC inherits the fast power/current dynamic response from the DPC method achieved by hysteresis current controllers. Also, it enjoys a lower current THD and fewer power ripples due to its current component's regulation. These features are obtained from the VC method. However, the method needs information of grid voltage and the calculation of VF [13], [14]. It should be noted that PWM and table-based methods steady-state performance comparisons are dependent on sampling and switching frequencies [15].

The measuring device failure or malfunction is also inevitable in the GCCs. Therefore, it is better to reduce the number of sensors to enhance the resiliency of the system and reduce the cost of converter-based renewable power generation. In this regard, several sensorless voltage estimation schemes have been proposed, which usually estimate the positive sequence of the voltage. But a few studies could be found in which estimating the unbalanced voltage conditions has been proposed while the LVRT capability is not considered at them [16], [17]. It is desirable to estimate the grid voltage under balanced and unbalanced conditions while the LVRT techniques are considered.

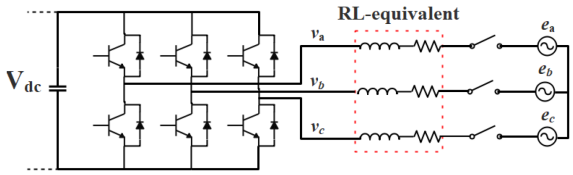


Fig. 1. Topology of a grid-connected voltage source converter.

In this article, a sensorless CC is proposed for GCCs. The following contributions are provided.

1) Resiliency enhancement:
   a) The method can tackle multiple risks, including unbalanced grid conditions, severe load changes, and faults.
   b) The VF estimation is eliminated; thus, the parameter dependence of the method is reduced. As a result, the GCC resiliency is improved against the system parameter variations.
   c) A grid voltage estimation is considered to enhance its resiliency against voltage sensor malfunctions.
2) Performance improvement:
   a) The proposed CC method has a better steady-state response than DPC due to the current regulations.
   b) The proposed CC method has a faster dynamic response than VC due to using hysteresis current controllers and being a table-based method.
   c) The proposed method calculates the current references to optimize the grid current THD in real-time.

The principles of the conventional CC method under normal grid conditions and improved CC for unbalanced grid conditions are reviewed in Section II. The proposed sensorless control method is introduced in Section III. In addition, a comparative analysis of the performance of GCC under conventional and proposed control methods is presented by extensive simulations and experimental results in Section IV. Finally, Section V concludes this article.

## II. System Model and Conventional CC

The main task of a GCC is to exchange the maximum available power with the highest possible power quality with the power grid taking into account the grid code requirements. By considering the converter as a voltage source, the simplified equivalent circuit of the GCC can be shown in Fig. 1 and its mathematical model is

$$e = Ri + L\frac{di}{dt} + v \tag{1}$$

where $e$ and $v$ are the grid and the converter voltage vectors, respectively, and $R$ and $L$ are the equivalent series resistance and inductance, respectively. In GCC applications, the line filter equivalent $R$ and $L$ are assumed as stator resistance and leakage inductance of a virtual ac machine, respectively. Thus, the grid voltage $e$ is induced by a virtual air gap flux linkage [18], [19]. Therefore, grid flux linkage $\lambda_e$ and converter flux linkage $\lambda_v$ can be expressed similar to the flux linkage definitions in an

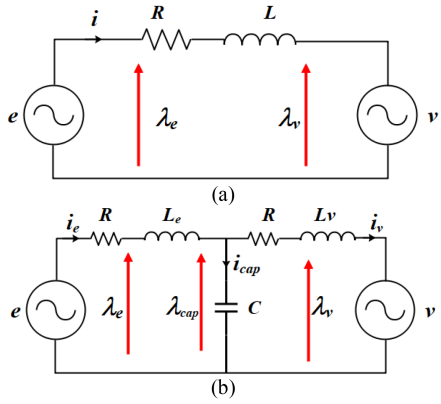


Fig. 2. Equivalent circuit of a grid-connected voltage source converter. (a) With *L* filter. (b) With *LCL* filter.

electrical machine as

$$\lambda_e = \int e dt \tag{2}$$

$$\lambda_v = \int v dt. \tag{3}$$

According to (1), $\lambda_e$ is rewritten as

$$\lambda_e = \int (v + Ri) dt + Li. \tag{4}$$

In reality, the value of *R* is negligible compared to the equivalent inductance value. Therefore, according to (2)–(4), the relationship between $\lambda_e$ and $\lambda_v$ is presented as

$$\lambda_e = \lambda_v + Li. \tag{5}$$

Different control methods based on VC and DPC with different control targets have been proposed in the literature for GCCs with their own merits and demerits. CC of VC and DPC was provided in order to have a control system that enjoys some positive advantages of either of the two basic methods, in addition to avoiding some of their drawbacks. The basics of CC method for both GCCs and electrical machines have been studied and proven [20], [21], [22]. The CC method is based on the proportionality of the *P* and *Q* changes to the currents and flux linkages components changes, which could be expressed as

$$\left.\begin{cases} \Delta P \propto \Delta i_q, \\ \Delta Q \propto \Delta i_d, \\ \Delta P \propto \Delta \lambda_{v_q}, \\ \Delta Q \propto \Delta \lambda_{v_d}, \end{cases}\right\} \cdots \Rightarrow \begin{cases} \Delta i_d = \frac{-1}{L} \Delta \lambda_{v_d} \\ \Delta i_q = \frac{-1}{L} \Delta \lambda_{v_q} \end{cases}. \tag{6}$$

CC method controls the currents through hysteresis controllers instead of PI ones and has a switching table instead of a PWM generator. In the topology shown in Fig. 1, the converter connects the grid through an equivalent *L* filter. It is also possible to use an *LCL* filter in order to attenuate the harmonics and reduce the filter size compared to the *L* filter. Fig. 2(a) and (b) show the equivalent circuit of a GCC with *L* and *LCL* filters, respectively. If the *LCL* filter is used instead of a series inductor, the VF estimation should be modified, as explained in the following [23], [24]. In this topology, the capacitor VF $\lambda_{cap}$ is expressed as

$$\lambda_{cap} = \int v dt + L_v i_v. \tag{7}$$

The grid VF is then calculated based on the converter-side flux linkage and $\lambda_{cap}$ as

$$\lambda_e = \lambda_{cap} + L_e(i_v + i_{cap}) = \lambda_{cap} + L_e i_e. \tag{8}$$

It should be noted that the exchanged active and reactive power is controlled in the converter side. Therefore, the reactive power that is consumed by the *LCL* capacitor should be considered in the *Q* calculation. The capacitor reactive power is expressed as

$$Q_{cap} = 1.5(i_{\alpha\beta_{cap}} \otimes v_{\alpha\beta_{cap}}). \tag{9}$$

The conventional CC method is proposed for balanced grid conditions in GCC applications. However, the conventional CC does not provide good performance under unbalanced grid conditions. Under the unbalanced conditions, the grid current THD increases extremely and the active and reactive power will have oscillations with a frequency of twice the line frequency that may not satisfy the grid codes and standards requirements. These issues may reduce the capacitor lifetime and subsequently the GCC reliable operation level decreased. In the single-phase GCCs, these oscillations are reduced by choosing a high enough dc-link capacitor value, changing the inverter topology, etc. [5], [25], [26]. However, solving these issues in three-phase GCCs is totally different and unlike normal conditions, filters cause more fluctuations in unbalanced conditions and cannot eliminate or reduce the power fluctuations. Another CC method was proposed to overcome these problems while maintaining the advantages of CC under unbalanced conditions [27]. In this CC method, a new current references calculation is suggested as

$$\begin{cases} i_x^* = -\frac{\frac{2}{3}P^*\lambda_{eq}}{\omega(\lambda_{ed}\lambda_{ey}-\lambda_{eq}\lambda_x)} + \frac{\frac{4}{3}Q^*\lambda_{ey}}{\omega(\lambda_{ed}^2+\lambda_{eq}^2+\lambda_{ex}^2+\lambda_{ey}^2)} \\ i_y^* = \frac{\frac{2}{3}P^*\lambda_{ed}}{\omega(\lambda_{ed}\lambda_{ey}-\lambda_{eq}\lambda_{ex})} - \frac{\frac{4}{3}Q^*\lambda_{ex}}{\omega(\lambda_{ed}^2+\lambda_{eq}^2+\lambda_{ex}^2+\lambda_{ey}^2)} \end{cases}. \tag{10}$$

As seen in (10), the "+" and "−" sequence extractions of grid voltages and currents are eliminated from the current reference's calculation process compared to the most recently presented unbalanced control methods [5]. Current references are calculated in the grid VF frame in this CC method. Fig. 3 shows the schematic diagram of the CC method under unbalanced grid conditions in which the reference current is calculated by the VF. However, LVRT capability is not considered in this method.

## III. Proposed CC

Although by applying the CC method presented briefly in the previous section, the grid current THD and the *P* oscillations under the unbalanced conditions are reduced, first, the method needs a VF estimation process. As shown in Fig. 4, the grid and filter parameters are used in the VF estimation process. This may lead to incorrect flux estimation due to parameter variations. According to (10) and Fig. 3, this issue directly affects the

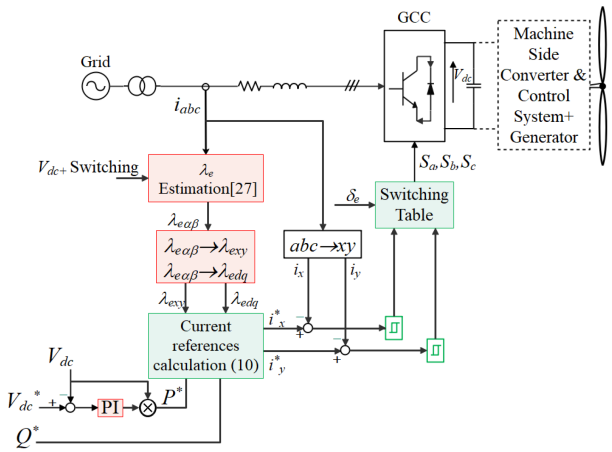


Fig. 3. Block diagram of the CC method under unbalanced grid conditions with the reference current calculated by a VF.

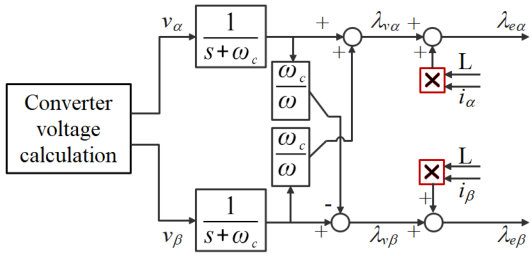


Fig. 4. Block diagram of the grid VF estimator.

current reference calculations, deteriorates the control system performance, and reduces the resilience of the system in both normal and abnormal conditions. Also, VF is usually presented for normal conditions, and its performance is not guaranteed in abnormal system conditions, such as faults in the grid, voltage sag at the point of common connection (PCC), or line parameter variations [28].

Second, according to Fig. 3 and (10), the CC method needs three different frame transformations, i.e., ($abc\rightarrow\alpha\beta$), ($\alpha\beta\rightarrow dq$), and ($\alpha\beta\rightarrow xy$). The mentioned CC method uses the grid VF angle for these frame transformations, which its uncertainty due to parameter variations and abnormal grid conditions could threaten the system resiliency. Also, it seems that applying improved PLL methods increases the computational burden and complexity of the system. Third, the presented CC method in Section II cannot respond under fault conditions. Also, software considerations are not provided for inverter protection against the overcurrent of the semiconductors. Therefore, the following control method is proposed based on the CC in order to control the system with improved power quality under balanced and unbalanced conditions. The VF estimation and different frame transformations are eliminated from the proposed CC method. Also, it is capable of responding against multiple risks. In the following, the principles of the proposed CC method are presented.

### A. Principles of the Proposed CC Method for Unbalanced Conditions

As presented in the previous section, under unbalanced conditions, the active and reactive powers have oscillations with a frequency of twice the line frequency in addition to a dc component as

$$\begin{cases} P = P_0 + P_{c2}\cos(2\omega t) + P_{s2}\sin(2\omega t) \\ Q = Q_0 + Q_{c2}\cos(2\omega t) + Q_{s2}\sin(2\omega t) \end{cases}. \tag{11}$$

It is common to use the "+" and "−" sequence components of $i$ and $e$ to expand (8). However, in the proposed CC method, the 90 electrical degrees lags components are used instead of "+" and "−" sequence components. Therefore, (11) could be expanded as

$$\begin{cases} P_0 = 3/4\left(i_{\alpha\beta}\odot e_{\alpha\beta} + i'_{\alpha\beta}\odot e'_{\alpha\beta}\right) \\ Q_0 = 3/4\left(i_{\alpha\beta}\otimes e_{\alpha\beta} + i'_{\alpha\beta}\otimes e'_{\alpha\beta}\right) \end{cases} \tag{12}$$

$$\begin{cases} \tilde{P}_{out} = 3/4\left(\left(i_{\alpha\beta}\odot v_{\alpha\beta} - i'_{\alpha\beta}\odot v'_{\alpha\beta}\right)\cos(2\omega t) \right. \\ \qquad \left. + \left(i_{\alpha\beta}\odot v'_{\alpha\beta} + i'_{\alpha\beta}\odot v_{\alpha\beta}\right)\sin(2\omega t)\right) \\ \tilde{Q}_{out} = 3/4\left(-\left(i_{\alpha\beta}\odot v'_{\alpha\beta} + i'_{\alpha\beta}\odot v_{\alpha\beta}\right)_2\cos(2\omega t) \right. \\ \qquad \left. + \left(i_{\alpha\beta}\odot v_{\alpha\beta} - i'_{\alpha\beta}\odot v'_{\alpha\beta}\right)_1\sin(2\omega t)\right) \end{cases} \tag{13}$$

where $F'_{\alpha\beta}$ denotes their quadrature values that lag $F_{\alpha\beta}$ by 90 electrical degrees. Under unbalanced conditions, it is required to minimize the active power oscillations. Also, the active power dc component of GCC should be adjusted to its reference value, i.e.,

$$\begin{cases} \bar{P} = \mathrm{P_{ref}} \\ \bar{Q} = Q_{\mathrm{ref}} \\ \tilde{P}_{\mathrm{out}} \simeq 0 \end{cases}. \tag{14}$$

According to (12), (13), and by solving (14), the current reference is calculated as

$$\begin{cases} i^*_\alpha = \frac{-4P^*}{3\Delta}\left[e'_\beta\ X_\beta + e_\alpha Y + e'_\alpha Z\right] + \frac{4Q^*}{3\Delta}\left[e'_\alpha\ X_\alpha - e_\beta Y - e'_\beta Z\right] \\ i^*_\beta = \frac{4P^*}{3\Delta}\left[e'_\alpha\ X_\alpha + e_\beta Y + e'_\beta Z\right] + \frac{4Q^*}{3\Delta}\left[e'_\beta\ X_\beta - e_\alpha Y - e'_\alpha Z\right] \end{cases} \tag{15}$$

where

$$\begin{cases} X_{\alpha\beta} = \left(v^2_{\alpha\beta} + v'^2_{\alpha\beta}\right) \\ Y = \left(v'_\alpha v_\beta - v_\alpha v'_\beta\right) \\ Z = \left(v_\alpha v_\beta + v'_\alpha v'_\beta\right) \end{cases}. \tag{16}$$

The current reference calculations of (15), compared to the conventional reference calculations (10), have the following advantages.

1) The VF components are eliminated.
2) The ($\alpha\beta\rightarrow dq$) and ($\alpha\beta\rightarrow xy$) reference frame transformations are eliminated.

On the other hand, it is required to achieve a sinusoidal grid current with an acceptable THD under unbalanced conditions. Although applying the current references (15) to the converter reduces the current THD, it does not guarantee a minimum current THD. Therefore, finding a simple, implementable relation between the current THD, $P$, and $Q$ is necessary to calculate

the references and improve the current THD. Various THD estimation methods have been proposed in the literature [29], [30]. The following THD estimation is online, does not have training time, has high accuracy, low computational burden, and does not need extra signals and parameters. It is presented as

$$\text{THD} = \frac{\sqrt{\sum_{n=2}^{\infty} I_n^2}}{I_1} = \sqrt{\frac{\|I_h\|^2}{\|I_f\|^2}} \tag{17}$$

where $I_f$ and $I_h$ are fundamental and harmonic current components, respectively. By assuming a sinusoidal phase voltage, the dc and ac components of $P$ and $Q$ for one phase are expressed as

$$\begin{cases} \bar{P} = 2EI_1 \cos(\theta_{e1} - \theta_{i1})\, s \\ \bar{Q} = 2EI_1 \sin(\theta_{e1} - \theta_{i1}) \end{cases} \tag{18}$$

$$\begin{cases} \tilde{P} = e\left[\sum_{n=2}^{\infty} \sqrt{2} I_n \cos(n\omega t + \theta_{in})\right] \\ \quad + e'\left[\sum_{n=2}^{\infty} \sqrt{2} I_n \cos\left(n\omega t + \theta_{in} - \frac{n\pi}{2}\right)\right] \\ \tilde{Q} = -e'\left[\sum_{n=2}^{\infty} \sqrt{2} I_n \cos(n\omega t + \theta_{in})\right] \\ \quad + e\left[\sum_{n=2}^{\infty} \sqrt{2} I_n \cos\left(n\omega t + \theta_{in} - \frac{n\pi}{2}\right)\right] \end{cases}. \tag{19}$$

$I_f$ and $I_h$ and their lagged values are calculated by

$$\begin{bmatrix} i_f \\ i'_f \end{bmatrix} = G \begin{bmatrix} e & -e' \\ e' & e \end{bmatrix} \begin{bmatrix} \bar{P} \\ \bar{Q} \end{bmatrix} \tag{20}$$

$$\begin{bmatrix} i_h \\ i'_h \end{bmatrix} = G \begin{bmatrix} e & -e' \\ e' & e \end{bmatrix} \begin{bmatrix} \tilde{P} \\ \tilde{Q} \end{bmatrix} \tag{21}$$

where

$$G = \frac{1}{e^2 + e'^2} \tag{22}$$

and $i'_{f \text{ and } h}$ denote their quadrature values that lag $i_{f \text{ and } h}$ by 90 electrical degrees. As seen in (18) and (19), the dc components are related to $I_f$ and the ac components are related to $I_h$. The rms of fundamental and harmonic components is expressed, respectively, as

$$\|I_f\|^2 = i_f^2 + i'^2_f \tag{23}$$

$$\|I_h\|^2 = i_h^2 + i'^2_h \tag{24}$$

where $I_h$ contains dc and ac components. The ac components should be eliminated, which is done by using a low-pass filter. Also, according to (20) and (21), the rms of fundamental and harmonic components is rewritten as

$$\|I_f\|^2 = \frac{\bar{P}^2 + \bar{Q}^2}{e^2 + e'^2} \tag{25}$$

$$\|I_h\|^2 = \frac{\tilde{P}^2 + \tilde{Q}^2}{e^2 + e'^2}. \tag{26}$$

Therefore, according to (17), (25), and (26), the current THD is expressed as

$$\text{THD} = \frac{\sqrt{\sum_{n=2}^{\infty} I_n^2}}{I_1} = \sqrt{\frac{\|I_h\|^2}{\|I_f\|^2}} = \sqrt{\frac{\tilde{P}^2 + \tilde{Q}^2}{\bar{P}^2 + \bar{Q}^2}}. \tag{27}$$

Equation (27) shows that minimizing the ac components of $P$ and $Q$ reduces the current THD. Also, the excess capacity of the converter can be assigned to dc components of $Q$ in order to improve the current THD. The reference $\bar{P}$ is determined according to the grid demand. Therefore, the second statement of (14) is expressed as

$$\bar{Q} = KQ_{ref}. \tag{28}$$

Conventionally, $K$ factor was chosen to be one. However, through different simulation and experimental tests presented in the next section, it is realized that setting $K = 1$ does not necessarily result in a minimum grid current THD. Therefore, according to the CC principles, (12), (13), and solving by (14), the current references can be found as

$$\begin{cases} i^*_\alpha = K_1\left(\frac{-4P^*}{3\Delta}\left[e'_\beta\, X_\beta + e_\alpha Y + e'_\alpha Z\right]\right. \\ \quad \left. + \frac{4Q^*}{3\Delta}\left[e'_\alpha\, X_\alpha - e_\beta Y - e'_\beta Z\right]\right) = K_1 i^*_{\alpha,con} \\ i^*_\beta = K_2\left(\frac{4P^*}{3\Delta}\left[e'_\alpha\, X_\alpha + e_\beta Y + e'_\beta Z\right]\right. \\ \quad \left. + \frac{4Q^*}{3\Delta}\left[e'_\beta\, X_\beta - e_\alpha Y - e'_\alpha Z\right]\right) = K_2 i^*_{\beta,con} \end{cases} \tag{29}$$

where $i^*_{\alpha\beta,con}$ denotes the current references presented in (15). Therefore, the optimized current reference according to the minimum THD is set, as shown in Fig. 5. According to this figure, first $i^*_{\alpha\beta,con}$ is calculated by (15), then $i^*_{\alpha\beta,con}$ and its lagged vector are multiplied by $K_1$ and $K_2$. After that, the dc and ac components of $P$ and $Q$ are calculated. Then, the current THD is calculated by (27). In the next step, $K_{1,2}$ are changed and the process is repeated. Finally, $K_{1,2}$ corresponding to the minimum current THD are selected. In selecting $K_{1,2}$, the power factor is also checked in order not to exceed the grid code standard.

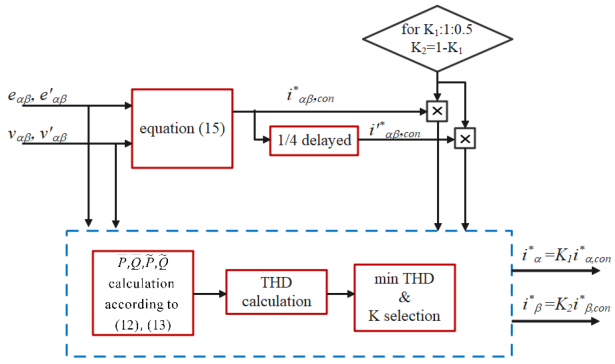


Fig. 5. Synthetize of the proposed current reference calculations.

## B. Sensorless CC

As presented in Section II, the resilience concept contains different aspects. Measuring equipment failure is one of the aspects that may threaten the system stable and reliable operation. Therefore, a state estimator and a disturbance observer are designed and added to the proposed CC method to reduce the number of sensors and enhance the resilience of the system. In the following, the principles of the observer are presented. The state-space equations of the system under the unbalanced

conditions become

$$\underbrace{\frac{d}{dt}\begin{bmatrix} i_d^+ \\ i_q^+ \\ i_d^- \\ i_q^- \end{bmatrix}}_{\dot{x}(t)} = \underbrace{\begin{bmatrix} -R/L & \omega & 0 & 0 \\ -\omega & -R/L & 0 & 0 \\ 0 & 0 & -R/L & -\omega \\ 0 & 0 & \omega & -R/L \end{bmatrix}}_{A_c} \underbrace{\begin{bmatrix} i_d^+ \\ i_q^+ \\ i_d^- \\ i_q^- \end{bmatrix}}_{x(t)} + \underbrace{\begin{bmatrix} 1/L & 0 & 0 & 0 \\ 0 & 1/L & 0 & 0 \\ 0 & 0 & 1/L & 0 \\ 0 & 0 & 0 & 1/L \end{bmatrix}}_{B_c} \underbrace{\begin{bmatrix} v_d^+ \\ v_q^+ \\ v_d^- \\ v_q^- \end{bmatrix}}_{u(t)} + \underbrace{\begin{bmatrix} 1/L & 0 & 0 & 0 \\ 0 & 1/L & 0 & 0 \\ 0 & 0 & 1/L & 0 \\ 0 & 0 & 0 & 1/L \end{bmatrix}}_{E_c} \underbrace{\begin{bmatrix} e_d^+ \\ e_q^+ \\ e_d^- \\ e_q^- \end{bmatrix}}_{d(t)} \tag{30}$$

$$y = C_c x(t), \qquad C_c = \begin{bmatrix} 1 & 0 & 0 & 0 \\ 0 & 1 & 0 & 0 \\ 0 & 0 & 1 & 0 \\ 0 & 0 & 0 & 1 \end{bmatrix}. \tag{31}$$

For the digital implementation, (30) and (31) should be transformed into the discrete-time model as

$$\begin{cases} x(k+1) = A_{dis}x(k) + B_{dis}u(k) + E_{dis}d(k) \\ y(k) = C_{disx}(k) \end{cases} \tag{32}$$

where

$$A_{dis} = I_{4\times4} + A_c T_s, \quad B_{dis} = B_c T_s, \qquad E_{dis} = E_c T_s. \tag{33}$$

The unknown grid voltage ($k$) is assumed to be constant, i.e.,

$$\dot{d}(t) = \begin{bmatrix} 0 & 0 & 0 & 0 \end{bmatrix}^T, \text{ or in discrete format: } d(k+1) = d(k) \tag{34}$$

in order to estimate the grid voltage, the state vector is combined with the grid voltage as a disturbance state

$$\begin{bmatrix} x(k+1) \\ d(k+1) \end{bmatrix} = \underbrace{\begin{bmatrix} A_{dis} & E_{dis} \\ 0 & I_{4\times4} \end{bmatrix}}_{A_m} \begin{bmatrix} x(k) \\ d(k) \end{bmatrix} + \underbrace{\begin{bmatrix} B_{dis} \\ 0 \end{bmatrix}}_{B_m} u(k) \tag{35}$$

$$y(k) = \begin{bmatrix} C_{dis} & 0 \end{bmatrix} \begin{bmatrix} x(k) \\ d(k) \end{bmatrix}. \tag{36}$$

The state ($k$) and disturbance ($k$) vectors are estimated based on the measurement of the grid currents. The proposed state and disturbance observer are expressed as

$$\underbrace{\begin{bmatrix} \hat{x}(k+1) \\ \hat{d}(k+1) \end{bmatrix}}_{\hat{M}(k+1)} = \underbrace{\begin{bmatrix} A_{dis} & E_{dis} \\ 0 & I_{4\times4} \end{bmatrix}}_{A_m} \underbrace{\begin{bmatrix} \hat{x}(k) \\ \hat{d}(k) \end{bmatrix}}_{\hat{M}(k)} + \underbrace{\begin{bmatrix} B_{dis} \\ 0 \end{bmatrix}}_{B_m} u(k) - \underbrace{\begin{bmatrix} L_1 \\ L_2 \end{bmatrix}}_{L_m} \underbrace{\begin{bmatrix} C_{dis} & 0 \end{bmatrix}}_{C_m} \underbrace{\begin{bmatrix} \hat{x}(k) \\ \hat{d}(k) \end{bmatrix}}_{\hat{M}(k)}. \tag{37}$$

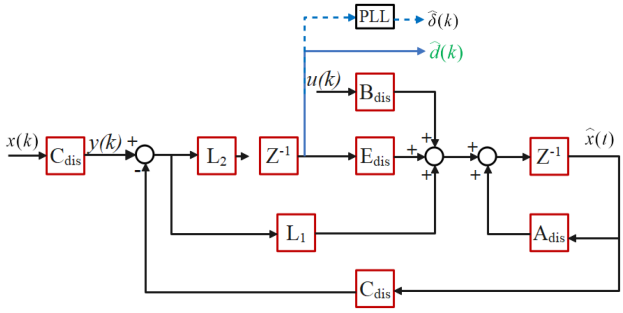


Fig. 6. Block diagram of state and disturbance observer to estimate grid voltages.

To determine the optimal observer gain $L_{\mathrm{m}}$, an error dynamic can be obtained by subtracting (37) from (35) as

$$\varepsilon_m = M(K+1) - \hat{M}(K+1) = \begin{bmatrix} A_{dis} - L_1 C_{dis} & E_{dis} \\ -L_2 C_{dis} & I_{4\times4} \end{bmatrix}. \tag{38}$$

The system in (37) is stable if, and only if, the following inequalities hold as

$$\begin{bmatrix} \delta H & (A_m - L_m C_m)^T \\ (A_m - L_m C_m) & H \end{bmatrix} > 0 \tag{39}$$

where $H$ is a positive-definite matrix, $\delta$ determines the convergent speed of the system states (39) can be solved using MATLAB LMI toolbox, taking into account the following constraints:

$$\begin{aligned} &\text{minimize } H \text{ subjected to (39)} \\ &\text{objects:} \\ &\quad \delta > 0 \\ &\quad H > 0 \\ &\quad HL_m > 0. \end{aligned} \tag{40}$$

Fig. 6 shows the block diagram of the state and disturbance observer used in the proposed CC method to estimate the grid voltage under balanced and unbalanced conditions.

### C. Faults

As presented in Sections I and II, balanced and unbalanced voltage dips may cause grid problems, such as voltage flickers, power outages, and system instability. Therefore, GCCs control methods should have LVRT capability to interact with the grid. Thus, the LVRT capability is considered in the proposed control method to have an appropriate response beyond just unbalanced conditions to enhance the resiliency of the system against multiple risks. In the design of the proposed method, short-circuit faults and extreme load changes are considered. According to the IEEE 1574 and the common advanced grid codes, the reactive power reference is set as

$$Q^* = \begin{cases} P_{nom} & 0 \le V_{pcc} < 0.5 \\ 2P_{nom}(1 - V_{pcc}) & 0.5 \le V_{pcc} < 0.9 \\ 0 & 0.9 \le V_{pcc} < 1.1 \end{cases}. \tag{41}$$

Under normal conditions, it is not required to inject any reactive power. Also, under abnormal grid conditions, the GCC

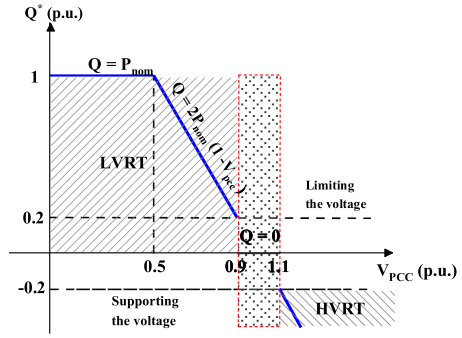


Fig. 7. Reactive power injection to support/limit the PCC voltage during LVRT.

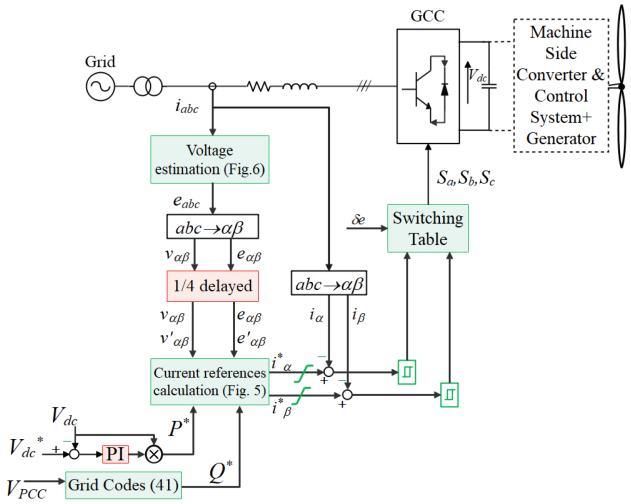


Fig. 8. Block diagram of the proposed CC method.

injects a required amount of reactive power according to (41) and Fig. 7 to improve the grid stability.

Fig. 8 shows a block diagram of the proposed CC method in which the grid voltage sensors are eliminated, and a grid voltage estimator is added to the system. This voltage estimator is appropriate for balanced and unbalanced conditions. Also, the reference current is calculated without using VF and optimized to achieve the minimum grid current THD. As shown in this figure, the VF estimator is eliminated and the reactive power reference is set according to the grid codes. The proposed CC method can provide an active power with high quality under both balanced and unbalanced conditions with an acceptable current THD. Also, during faults that cause voltage dips, the injected current to the grid increases to provide desired active and reactive power. This may cause damage to the converter due to the semiconductor over current. Therefore, a current limiting strategy is also considered for enhancing LVRT operation of the GCC.

## IV. Performance Analysis

In this section, the performance of the proposed CC method is investigated by performing several simulation and experimental tests. The proposed CC performance is compared with the conventional CC presented in Section II under grid balanced, unbalanced conditions, and voltage sag caused by the fault. The system parameters are listed in Table I.

TABLE I
System Parameters

| System Parameters | Value |
|---|---|
| Equivalent resistance (R) | 0.3 Ω |
| Equivalent impedance (L) | 15 mH |
| Capacitor of dc link (C) | 3.76 mF |
| Voltage frequency (f) | 50 HZ |

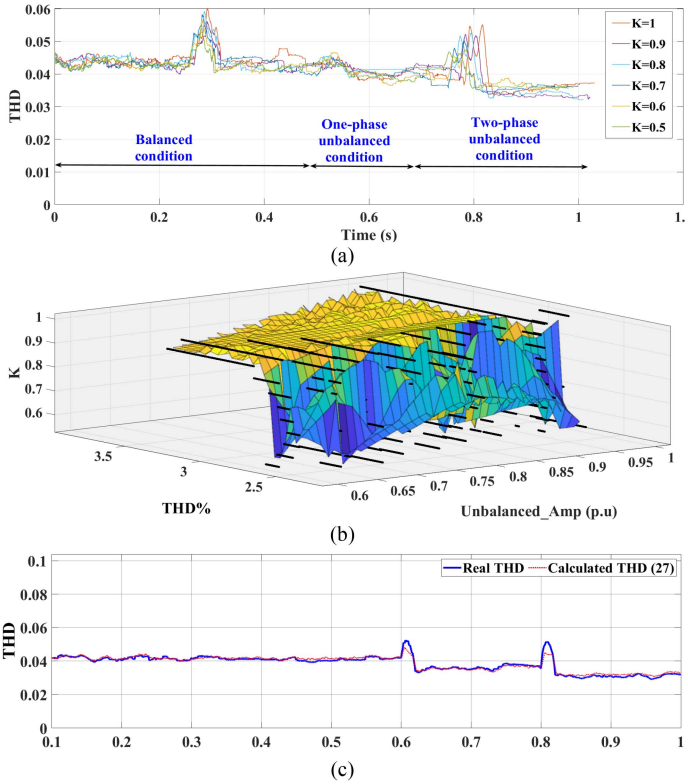


Fig. 9. (a) and (b) Effects of the $K$ factor variation on the current THD. (c) Validation of calculated THD by (27) with real THD.

As presented in Section III-A, $K_{1,2}$ is investigated and the results are illustrated in Fig. 9. In this figure, $K$ is represented as $K_1$ in (29) and $K_2$ is assumed to be $1\text{-}K_1$. Fig. 9(a) shows the current THD under three different conditions: 1) before $t = 0.5$ s, the grid voltages are balanced, 2) at $t = 0.5$ s, the voltage magnitude of phase-c drops by 20%, 3) the transition from one-phase to two-phase unbalanced conditions occurs at $t = 0.7$ s. Also, $K$ varies from 1 to 0.5 by steps of 0.1. As seen in Fig. 9(a), no specific $K$ minimizes the current THD under any conditions. In order to deepen the study of the effect of $K$, the voltage drops vary from 100% to 60% in one-phase by steps of 5%, and K varies from 1 to 0.5 by steps of 0.01. The current THD corresponding to the variations is shown in Fig. 9(b). Fig. 9(c) shows the validation of calculated THD by (27) with real THD. As shown in Fig. 9(c), the calculated THD and the real one are very close. Also, two active power reference changes at $t = 0.6$ s and $t = 0.8$ s are applied to the system to investigate the validation of calculated THD in this kind of condition.

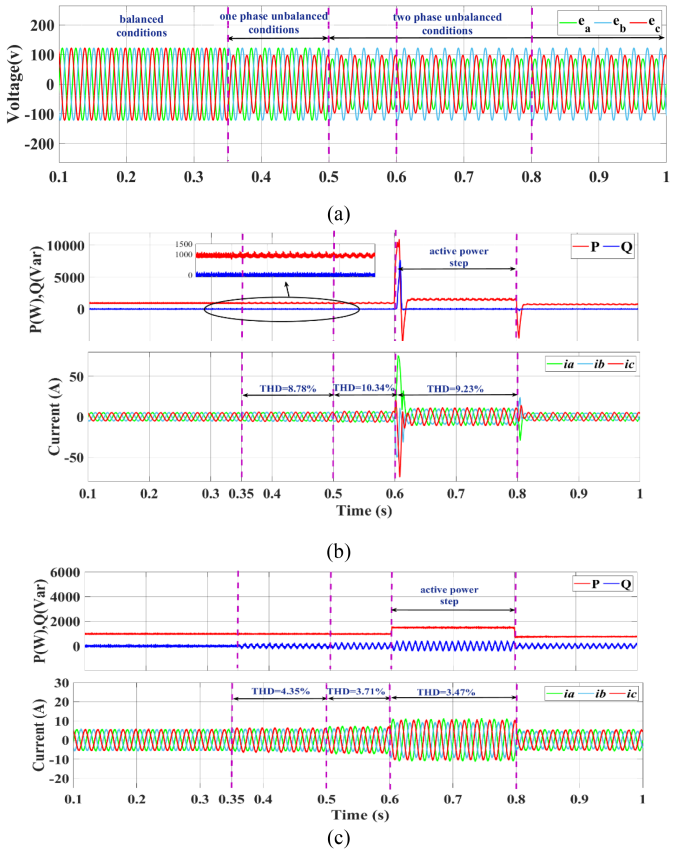


Fig. 10. Simulation results under two-phase unbalanced grid conditions. (a) Grid voltages. (b) Conventional CC method. (c) Proposed CC method.

The transition from one-phase to two-phase unbalanced conditions under the two control methods is studied and their simulation results are presented in Fig. 10. The grid operates normally up to $t = 0.35$ s. At $t = 0.35$ s, the voltage magnitude of phase-c drops by 20%, and after the transition from one-phase to two-phase unbalanced condition, which occurs at $t = 0.5$ s, the $P$ and $Q$ oscillations of the conventional CC method increase and the current THD reaches to 10.34%, which is far away from the grid codes regarding THD limitations. However, it is seen that the $P$ oscillations are eliminated under the proposed CC method and the current THD reduces to about 3.7%. In addition, the dynamic performances of both control methods are investigated under unbalanced conditions. The active power reference of system under the control methods increases from 1000 to 1500 W at $t = 0.6$ s and decreases from 1500 to 700 W at $t = 0.8$ s, respectively. As seen in Fig. 10(b) and (c), the system under the conventional CC method has a big overshoot in $P$, $Q$, and currents under dynamic conditions. However, the active power follows its reference appropriately in the system when the proposed CC method is used.

The performance of the conventional and proposed CC methods is investigated under two voltage sags at the PCC. The results are presented in Fig. 11, respectively. First, the PPC voltage drops by 45% at $t = 0.4$ s and last for 0.2 s. It then drops by 20% at $t = 0.8$ s and lasts 1 s. As shown in Fig. 11(a), the conventional CC cannot support the PCC voltage. However, the proposed CC method injects a specific amount of reactive power to support

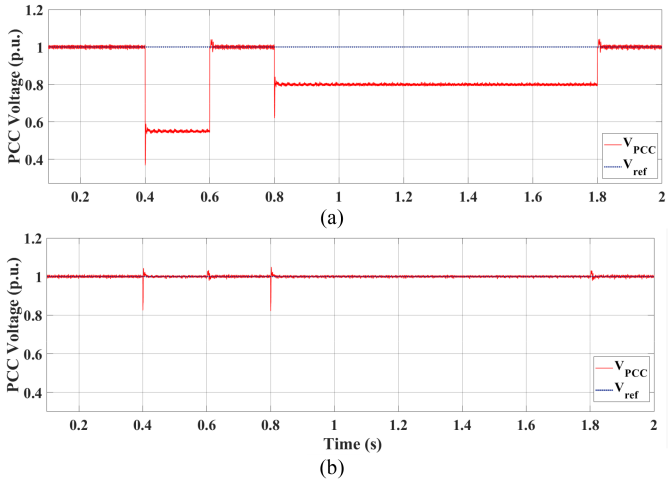


Fig. 11. PCC voltage in per-unit for LVRT test. (a) Conventional CC method. (b) Proposed CC method.

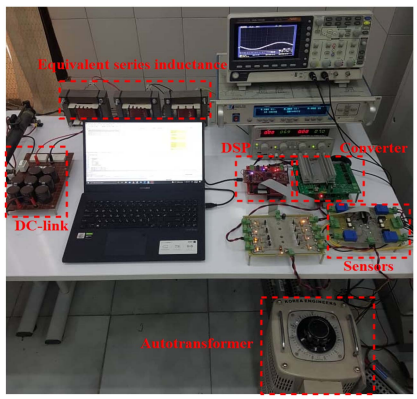


Fig. 12. Picture of the experimental setup.

TABLE II
SPECIFICATIONS OF EXPERIMENTAL SETUP

| System Parameters | Value |
|---|---|
| Line-line voltage (e) | 50 V |
| Voltage frequency (f) | 50 HZ |
| Equivalent inductance (L) | 15.29 mH |
| Equivalent resistance (R) | 0.5 Ω |
| Capacitor of DC link (C) | 3.76 mF |
| DC-link voltage | 110 V |
| Sampling frequency | 20 KHz |
| Average switching frequency of proposed CC method | 5.6 KHz |
| Imbalance percentage | 15% |

the PCC voltage. The performance of the proposed CC method is shown in Fig. 11(b).

Experimental tests are performed to confirm the effectiveness of the proposed control method. The conventional and proposed CC under balanced and unbalanced grid voltage conditions are tested. The experimental setup contains a TMS320F28379D to execute the proposed control method, which is shown in Fig. 12. The specifications of the experimental setup are listed in Table II.

Fig. 13(a) shows the phase voltage and its angle under the balanced conditions. The grid unbalance is around 15%, which is caused by adding a resistor between the grid and the inductance

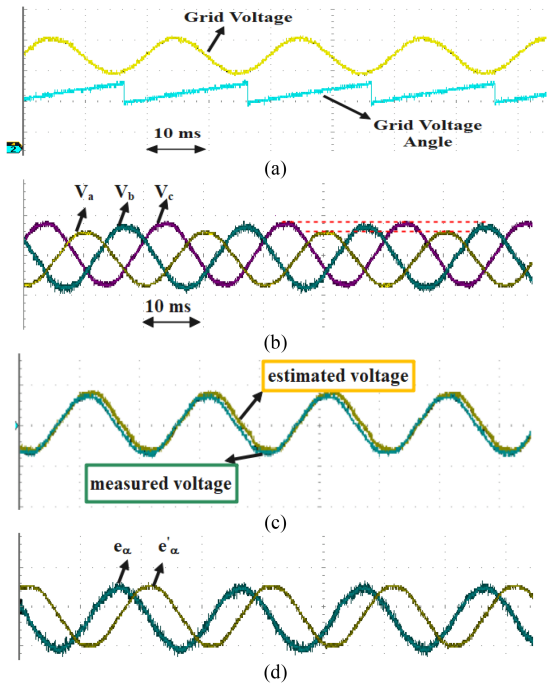


Fig. 13. Experimental results. (a) Grid voltage and its angle under balanced conditions. (b) One-phase unbalanced voltage conditions. (c) Estimated and measured voltage. (d) $e_\alpha$ and $e'_\alpha$ under unbalanced conditions.

in one phase during the experiment. Fig. 13(b) shows the result under the unbalanced condition. Fig. 13(c) shows the measured and estimated grid voltages. Also, Fig. 13(d) shows $e'_\alpha$ that lags by 90 electrical degrees.

Fig. 14(a) and (b) show the active and reactive power under unbalanced conditions for the conventional and the proposed CC methods, respectively, by experimental tests. The results show the effectiveness of the proposed method in eliminating active power oscillations. Fig. 14(c) presents the experimental results for various grid active power under the proposed method for about 90 s. The dc-link voltage reference changes manually. Subsequently, the active power reference changes. It is seen that the proposed method follows the references fast and accurately under the grid normal conditions. Fig. 14(d) shows the zoomed $P$ and $Q$ dynamic response under unbalanced conditions of the proposed CC method, respectively, by experimental tests.

Fig. 15(a) and (b) present $P$, $I$, and fast Fourier transforms (FFTs) of current under unbalanced conditions for the conventional CC and the proposed CC method, respectively, by experimental tests. Active power oscillations are eliminated under the proposed CC method. However, the conventional CC causes $P$ oscillations. The current waveforms of the two methods with their FFT show that the proposed method has a much lower THD.

Fig. 16 presents the zoomed dynamic response of the conventional and proposed CC methods, respectively, by experimental tests. As explained in connection with Fig. 15, the GCC system with the conventional CC experiences active power oscillations. While the GCC system with the proposed CC does not

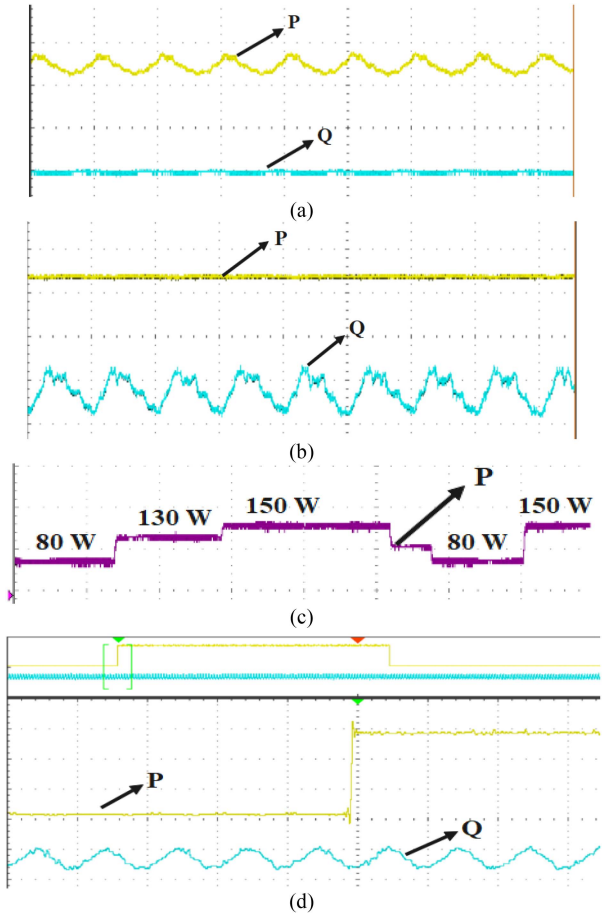


Fig. 14. Experimental results under the unbalanced conditions. (a) $P$ and $Q$ of conventional CC method. (b) $P$ and $Q$ of the proposed CC method. (c) Injecting various amounts of $P$ to the grid. (d) $P$ and $Q$ results of dynamic response for one-phase unbalanced grid conditions of the proposed CC method.

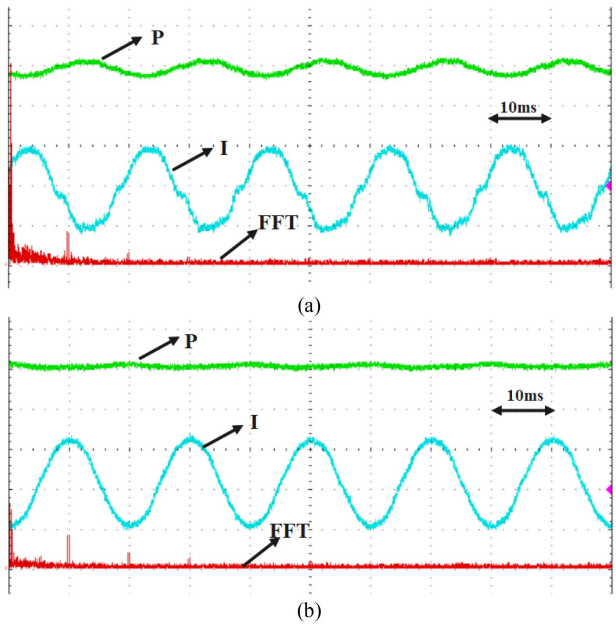


Fig. 15. Experimental results of $P$, $I$, and FFT of current under the unbalanced conditions. (a) Conventional CC method. (b) Proposed CC method.

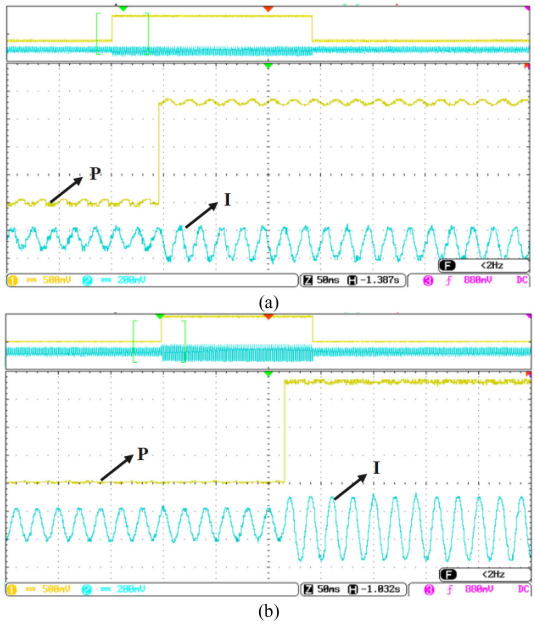


Fig. 16. *P* and *I* experimental results of dynamic response for one-phase unbalanced grid conditions. (a) Conventional CC method. (b) Proposed CC method.

cause active power oscillations and shows lower current THD compared to the conventional CC.

It is seen that the two sets of simulation and experimental results are in good agreement. As the simulation results are explained in Fig. 10, the steady-state performance of the conventional and the proposed CC methods under the unbalanced conditions has been investigated in the time interval of 0.35 to 0.6. As seen in Figs. 14(a), (b), and 15, same as the simulation results at steady-state, the conventional CC method has active power oscillations under the unbalanced conditions. However, *P* oscillations of the proposed CC are eliminated and this method has a much lower current THD as the current FFT shows in Fig. 15. Also, the dynamic performance of the two methods under the unbalanced conditions are investigated. The simulation results of dynamic performance under the unbalanced conditions are shown in Fig. 10. The experimental results of dynamic performance under the unbalanced conditions are shown in Figs. 14(c), (d), and 16. As seen in these figures, the simulation and experimental results are similar. Their little difference is due to the dc-link response. Thus, the effectiveness of the proposed CC can be validated.

A brief comparison of the conventional CC and the proposed method is presented as a bar chart in Fig. 17. Also, it seems necessary to mention that the real-time implementation of the proposed CC method is very similar to the DPC. The proposed method does not have the challenges of PI controller tunning compared to VC methods. Also, in the VF estimation, positive and negative sequence extractions of variables are not needed in the proposed CC method.

## V. Conclusion

An improved sensorless CC is proposed in this article for GCCs to enhance the resilience of the system in different aspects

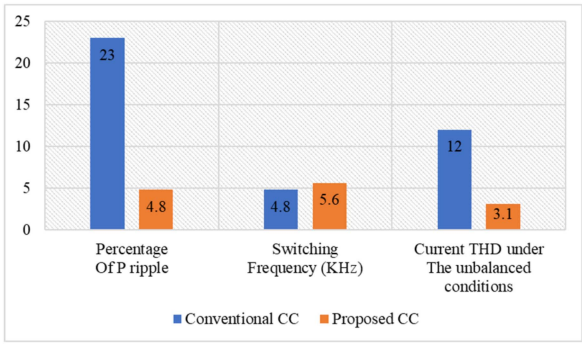


Fig. 17. Comparison of the conventional CC and the proposed method performances.

while the exchanged power quality of the system is improved. In term of system configuration, the current reference vector is obtained by optimizing the grid current THD without estimating a VF vector. Thus, the exchanged power quality is improved while the control system has less dependence on the grid and filter parameters and their variations. Also, the grid voltage estimation is used instead of the grid voltage sensing in order to reduce the risks of malfunction of sensors. Thus, the control system becomes more robust and reliable under different operating conditions. Compared to the common GCCs control under unbalance conditions, the proposed method avoids using a complex positive and negative sequence extraction of signals and avoids current PI controllers. In addition, it employs an active current limiter to prevent the converter failures caused by over currents. In term of performance, under normal and abnormal conditions, the proposed method well respects the corresponding grid standards. In addition, the system shows a good dynamic performance by tracking the active power references without abnormal overshoots. Furthermore, the proposed method improves power ripples and the current THD significantly compared to the conventional CCC by applying an intelligent reference calculator.

## References

[1] Global Wind Energy Council, "GWEC| global wind report 2021". [Online]. Available: https://gwec.net/wp-content/uploads/2021/03/GWEC-Global-Wind-Report-2021.pdf

[2] M. S. Eslahi, S. Vaez-Zadeh, and J. Rodriguez, "Combined control of grid connected converters for resiliency improvement of smart micro grids against multiple risks," in *Proc. IECON–47th Annu. Conf. IEEE Ind. Electron. Soc.*, 2021, pp. 1–6.

[3] S. Wang, P. Dehghanian, M. Alhazmi, and M. Nazemi, "Advanced control solutions for enhanced resilience of modern power-electronic-interfaced distribution systems," *J. Modern Power Syst. Clean Energy*, vol. 7, no. 4, pp. 716–730, 2019.

[4] Y. Zhang, J. Liu, H. Yang, and J. Gao, "Direct power control of pulsewidth modulated rectifiers without DC voltage oscillations under unbalanced grid conditions," *IEEE Trans. Ind. Electron.*, vol. 65, no. 10, pp. 7900–7910, Oct. 2018, doi: 10.1109/Tie.2018.2807421.

[5] S. F. Zarei, H. Mokhtari, M. A. Ghasemi, S. Peyghami, P. Davari, and F. Blaabjerg, "Control of grid-following inverters under unbalanced grid conditions," *IEEE Trans. Energy Convers.*, vol. 35, no. 1, pp. 184–192, Mar. 2020.

[6] M. Nasiri, J. Milimonfared, and S. H. Fathi, "A review of low-voltage ride-through enhancement methods for permanent magnet synchronous generator based wind turbines," *Renewable Sustain. Energy Rev.*, vol. 47, pp. 399–415, 2015, doi: 10.1016/j.rser.2015.03.079.

[7] M. M. Kabsha and Z. H. Rather, "Advanced LVRT control scheme for offshore wind power plant," *IEEE Trans. Power Del.*, vol. 36, no. 6, pp. 3893–3902, Dec. 2021.

[8] A. Khodaei, "Resiliency-oriented microgrid optimal scheduling," *IEEE Trans. Smart Grid*, vol. 5, no. 4, pp. 1584–1591, Jul. 2014.
[9] C. Chen, J. Wang, F. Qiu, and D. Zhao, "Resilient distribution system by microgrids formation after natural disasters," *IEEE Trans. Smart Grid*, vol. 7, no. 2, pp. 958–966, Mar. 2016.
[10] M. N. Ambia, K. Meng, W. Xiao, and Z. Y. Dong, "Comprehensive solution of networked microgrid towards enhanced overload resiliency," in *Proc. Int. Conf. Power Syst. Technol.*, 2018, pp. 1736–1742.
[11] Y. Gui, X. Wang, and F. Blaabjerg, "Vector current control derived from direct power control for grid-connected inverters," *IEEE Trans. Power Electron.*, vol. 34, no. 9, pp. 9224–9235, Sep. 2019.
[12] J. Hu and Z. Q. Zhu, "Improved voltage-vector sequences on dead-beat predictive direct power control of reversible three-phase grid-connected voltage-source converters," *IEEE Trans. Power Electron.*, vol. 28, no. 1, pp. 254–267, Jan. 2013, doi: 10.1109/Tpel.2012.2194512.
[13] Y. Cho and K.-B. Lee, "Virtual-flux-based predictive direct power control of three-phase PWM rectifiers with fast dynamic response," *IEEE Trans. Power Electron.*, vol. 31, no. 4, pp. 3348–3359, Apr. 2016, doi: 10.1109/Tpel.2015.2453129.
[14] J. Mohammadi, S. Vaez-Zadeh, E. Ebrahimzadeh, and F. Blaabjerg, "Combined control method for grid-side converter of doubly fed induction generator-based wind energy conversion systems," *IET Renewable Power Gener.*, vol. 12, no. 8, pp. 943–952, 2018.
[15] M. S. Eslahi, S. Vaez-Zadeh, and A. Jabbarnejad, "A comparative study of control methods for grid side converters in PMSG-based wind energy conversion systems," in *Proc. IEEE 29th Int. Symp. Ind. Electron.*, 2020, pp. 979–984.
[16] F. Benyamina, A. Benrabah, F. Khoucha, M. F. Zia, Y. Achour, and M. Benbouzid, "An augmented state observer-based sensorless control of grid-connected inverters under grid faults," *Int. J. Elect. Power Energy Syst.*, vol. 133, 2021, Art. no. 107222.
[17] N. N. Nam, N. D. Nguyen, C. Yoon, M. Choi, and Y. I. Lee, "Voltage sensorless model predictive control for a grid-connected inverter with LCL filter," *IEEE Trans. Ind. Electron.*, vol. 69, no. 1, pp. 740–751, Jan. 2022.
[18] A. M. Razali, M. A. Rahman, G. George, and N. A. Rahim, "Analysis and design of new switching lookup table for virtual flux direct power control of grid-connected three-phase PWM AC–DC converter," *IEEE Trans. Ind. Appl.*, vol. 51, no. 2, pp. 1189–1200, Mar./Apr. 2015.
[19] L. Xu, D. Zhi, and L. Yao, "Direct power control of grid connected voltage source converters," in *Proc. IEEE Power Eng. Soc. Gen. Meeting*, 2007, pp. 1–6.
[20] M. Jahanpour-Dehkordi, S. Vaez-Zadeh, and J. Mohammadi, "Development of a combined control system to improve performance of a PMSG based wind energy conversion system under normal and grid fault conditions," *IEEE Trans. Energy Convers.*, vol. 34, no. 3, pp. 1287–1295, Sep. 2019.
[21] A. Jabbarnejad, S. Vaez-Zadeh, and M. Jahanpour-Dehkordi, "Combined control of grid connected converters based on a flexible switching table for fast dynamic and reduced harmonics," *IEEE Trans. Energy Convers.*, vol. 35, no. 1, pp. 77–84, Mar. 2020.
[22] S. Vaez-Zadeh, *Control of Permanent Magnet Synchronous Motors*. London, U.K.: Oxford Univ. Press, 2018.
[23] M. A. Djema, M. Boudour, and A. A. Ladjici, "Direct power control modeling with optimized LCL filter for grid integrated renewables," in *Proc. 3rd Int. Conf. Control, Eng. Inf. Technol.*, 2015, pp. 1–6.
[24] V. R. Chowdhury, S. Mukherjee, P. Shamsi, and M. Ferdowsi, "Control of a three-phase inverter under unbalanced grid conditions," in *Proc. IEEE Energy Convers. Congr. Expo.*, 2017, pp. 2909–2913.
[25] P. T. Krein, R. S. Balog, and M. Mirjafari, "Minimum energy and capacitance requirements for single-phase inverters and rectifiers using a ripple port," *IEEE Trans. Power Electron.*, vol. 27, no. 11, pp. 4690–4698, Nov. 2012.
[26] Y.-M. Chen, C.-H. Chang, and H.-C. Wu, "DC-link capacitor selections for the single-phase grid-connected PV system," in *Proc. Int. Conf. Power Electron. Drive Syst.*, 2009, pp. 72–77.
[27] A. Jabbarnejad, S. Vaez-Zadeh, and M. Khalilzadeh, "Sensorless virtual flux combined control of grid connected converters with high power quality under unbalanced grid operation," *IEEE Trans. Sustain. Energy*, vol. 12, no. 2, pp. 785–793, Apr. 2021.
[28] A. Jabbarnejad, S. Vaez-Zadeh, and M. Khalilzadeh, "Virtual-flux-based DPC of grid connected converters with fast dynamic and high power quality," in *Proc. IECON-45th Annu. Conf. IEEE Ind. Electron. Soc.*, 2019, pp. 4031–4036.
[29] L. Wang, C.-S. Lam, and M.-C. Wong, "Total harmonic distortion (THD) estimation technique based on power concept for smart power meters," in *Proc. IEEE Power Energy Soc. Asia-Pacific Power Energy Eng. Conf.*, 2019, pp. 1–6.
[30] M. Comanescu, "Estimation of THD, harmonic components and power factor in three-phase rectifiers," in *Proc. IEEE Int. Conf. Ind. Technol.*, 2020, pp. 468–473.

**Mohammad Sadegh Eslahi** received the B.Sc. degree in electrical engineering from the University of Shiraz, Shiraz, Iran, in 2015, and the M.Sc. degree in electrical engineering from the K. N. Toosi University of Technology, Tehran, Iran, in 2017. He is currently working toward the Ph.D. degree in electrical engineering- power electronics with the Advanced Motion Systems Research Laboratory, University of Tehran, Tehran, Iran.

His research interests include power electronics, motor drives, control and dynamic analysis of power electronic systems, mainly distributed and grid-connected converters, and microgrids.

**Sadegh Vaez-Zadeh** (Senior Member, IEEE) received the B.Sc. degree in electrical engineering from the Iran University of Science and Technology, Tehran, Iran, in 1985, and the M.Sc. and Ph.D. degrees in electrical engineering from Queen's University, Kingston, ON, Canada, in 1993 and 1997, respectively.

In 1997, he joined the University of Tehran, Tehran, Iran, as an Assistant Professor and became an Associate Professor in 2001 and a Full Professor in 2005. Prior to this, he had been with several research and educational institutions in different positions. He was the Head of the Power Department, University of Tehran, where he is currently the Director of the Advanced Motion Systems Research Laboratory, which he founded in 1998. He has coauthored more than 200 research papers. He holds a U.S. patent. He is the author of the book entitled *Control of Permanent Magnet Synchronous Motors* (Oxford University Press, 2018) with its Chinese translation published in 2022. His research interests include advanced rotary and linear electric machines and drives, wireless power transfer, renewable energy integration, and energy policy.

Dr. Vaez-Zadeh is an Editor for the IEEE TRANSACTIONS ON SUSTAINABLE ENERGY and IEEE TRANSACTIONS ON ENERGY CONVERSION and a Subject Editor for the *IET Renewable Power Generation*. He has been active in IEEE-sponsored conferences as a General Chair, a Keynote Speaker, and a member of technical and steering committees. He is a Member of the Energy Internet Coordinating Committee, Motor Subcommittee, and Power System Stability Control Subcommittee of the IEEE Power and Energy Society. He was the recipient of several domestic and international awards for his contributions to the fields.

**Jose Rodriguez** (Life Fellow, IEEE) received the Engineer degree in electrical engineering from the Universidad Tecnica Federico Santa Maria, Valparaiso, Chile, in 1977, and the Dr.-Ing. degree in electrical engineering from the University of Erlangen, Erlangen, Germany, in 1985.

He has been with the Department of Electronics Engineering, Universidad Tecnica Federico Santa Maria, since 1977, where he was a Full Professor and President. From 2015 to 2019, he was the President of the Universidad Andres Bello, Santiago, Chile. Since 2022, he has been a President of the Universidad San Sebastian, Santiago, Chile. He has coauthored two books, several book chapters, and more than 700 journal and conference papers. His main research interests include multilevel inverters, new converter topologies, control of power converters, and adjustable-speed drives.

Dr. Rodriguez was the recipient of a number of best paper awards from journals of the IEEE. He is a member of the Chilean Academy of Engineering. He was the recipient of the National Award of Applied Sciences and Technology from the government of Chile in 2014. In 2015, he was also the recipient of the Eugene Mittelmann Award from the Industrial Electronics Society of the IEEE. From 2014 to 2022, he was included in the list of Highly Cited Researchers published by Web of Science.